

# Nonlinear modeling reveals multi-timescale and higher-order effects in active tissue mechanics

Chaozhen Wei<sup>1,\*</sup> and Min Wu<sup>1, 2, †</sup>

<sup>1</sup>Department of Mathematical Sciences, Worcester Polytechnic Institute, Worcester, MA 10605 USA

<sup>2</sup>Bioinformatics and Computational Biology, Worcester Polytechnic Institute, Worcester, MA 10605 USA

(Dated: March 18, 2021)

Cell proliferation, apoptosis, and myosin-dependent contraction can generate elastic stress and strain in living tissues, which may be dissipated by tissue rearrangement through cell topological transition and cytoskeletal reorganization. The present work demonstrates significant nonlinear effects in macroscopic tissue mechanics arising from the competition between force-generating and dissipating processes. We develop a mathematical model to describe the coupled dynamics of tissue activities and mechanics in the nonlinear regime. The model exhibits multi-timescale behavior when the timescale of rearrangement is much shorter than that of growth and constriction. Under this condition, tissue behaves like an active viscoelastic solid at the shorter timescale and like an active viscous fluid at the longer timescale. The accumulated prestrain due to growth and constriction can regulate its viscosity. We solve the full nonlinear system considering the local growth rate coupled with a chemical gradient within a 2D radially symmetric tissue region. We find that the elastic properties and rearrangement rate can regulate tissue size as a higher-order effect due to advection in tissue flow. Furthermore, we show that tissue mechanics' nonlinear effects can increase tissue size control sensitivity via mechanical feedback mechanisms.

Keywords: Differential growth | prestrain |nonlinear elasticity| tissue fluidity |mechanical feedback

## INTRODUCTION

The interaction between cell dynamics and tissue mechanics plays an essential role during development, homeostasis, and cancer progression [1–10]. Not only do cell activities generate mechanical forces that drive tissue flow and deformation [11, 12], they also respond to local stress and strain [13]. These mechanical cues can regulate cell proliferation and apoptosis through cell competition [1–3], contact inhibition [4–6], and mechanical feedback processes [7–10]. Recent experimental evidence shows that these processes share overlapping signaling pathways (e.g., Hippo signaling hubs and YAP/TAZ activity), while altered expression of their core components leads to tumorigenesis [14–17]. Interestingly, other experiments demonstrate that growing tumors also respond to the change of mechanical cues [18–20]. In light of the growing empirical evidence for the role of feedback mechanisms in living tissues, the present study seeks to improve our analytical understanding of tissue mechanics to better characterize tissue size regulation in both normal and abnormal conditions.

Cell activities such as proliferation, apoptosis, and myosin-dependent contractility can generate elastic stress and strain in the tissue, which can be dissipated through cell-cell topological transition [11, 12] and cytoskeleton reorganization [21]. Such rearrangements can occur collectively during epithelial tissue planar deformation and

confer a certain level of stress relaxation and fluidization to the elastic tissue [22, 23]. When force dissipation is assumed to be sufficiently rapid, previous studies have explained tissue as viscous fluid flow driven by the spatial gradient of myosin-dependent contractility [24, 25]. However, such models cannot describe how the dynamics of force generation and dissipation compete with each other to regulate tissue mechanics synergistically.

On the other hand, when force dissipation is not fast enough, a significant elastic strain can accumulate in the tissue. As revealed by tissue severance experiments on pupal thorax epithelia of *Drosophila*, tissue patches' size and shape can be far from their intrinsic stress-free state due to the stored myosin-dependent contraction [26, 27]. Limited by the assumption of infinitesimal elastic strains, previous linear models cannot explain how these measurable finite elastic strains and their associated stresses can arise [28–30]. More importantly, the potential nonlinear dynamics during the development of finite elastic strains and their interplay with tissue growth and constriction have not been explored.

This paper describes nonlinear tissue mechanics as a synergistic process arising from the competition between force-generating and force-dissipating activities. We further study the coupling effects of tissue mechanics with growth and constriction. To do so, we develop a nonlinear model to connect the dynamics of stress and strain with the activities of cell proliferation, apoptosis, myosin-dependent constriction, and tissue rearrangement. Then we study how tissue mechanics affect growth by considering how the growth rate is coupled with chemical gradients and mechanical cues. This approach is essentially different from traditional nonlinear elastic growth

\* cwei4@wpi.edu

† To whom correspondence should be addressed.  
E-mail: englier@gmail.com

theory [31, 32] where the local growth rate (or accumulated growth) is given an *a priori* functional form. Rather in our model, the accumulated growth emerges directly from the spatiotemporal dynamics of force-generating and dissipating activities. The present work also expands on our recent study where the tissue was assumed to be strictly incompressible [33]. Here we relax this assumption to allow the tissue patch area to evolve far from its intrinsic stress-free area due to accumulated constriction.

This paper is organized as follows. In the next section, we present the nonlinear elastic model that couples the dynamics of active tissue growth and constriction (force-generating activities) and adaptive rearrangement. We show the multi-timescale behavior of tissue in the linearized model when the timescale of rearrangement is shorter than that of force-generating activities. In such a regime, tissue behaves like a viscoelastic solid at the shorter timescale and like active viscous fluid at the longer timescale. The accumulated prestrain due to growth and constriction can regulate its viscosity. Then, we solve the full nonlinear system considering the local growth rate coupled with a chemical gradient within a 2D radially symmetric tissue region. We find that the elastic properties and rearrangement rate can regulate tissue size as a higher-order effect due to advection in tissue flow. Lastly, by coupling the local growth rate with mechanical feedback machinery, we show that tissue mechanics' nonlinear effects can increase tissue size variation sensitivity to the change of mechanical feedback strengths.

## GROWING TISSUES AS COMPRESSIBLE ELASTIC MATERIAL WITH REARRANGEMENT

### Growth, Constriction, and Elasticity

We describe the growth and elasticity of soft tissues in the Eulerian coordinates, denoted by  $\mathbf{x} \in \Omega$ . Let  $\mathbf{y} = \mathbf{Y}(\mathbf{x}, t)$  be the reference map, which relates the current and reference coordinates (respectively,  $\mathbf{x}$  and  $\mathbf{y}$ ) in the tissue [34, 35]. Then, the *geometric deformation tensor* is obtained as  $\mathbf{F} = \frac{\partial \mathbf{x}}{\partial \mathbf{y}} = \nabla \mathbf{Y}^{-1}$  (here  $\nabla = \nabla_{\mathbf{x}}$ ), and it can be decomposed as  $\nabla \mathbf{Y}^{-1} = \mathbf{F}_e \mathbf{P}$  [31]. Here,  $\mathbf{P}$  is the local accumulated *prestrain tensor* due to cell proliferation, apoptosis, or actomyosin-associated contractility, and  $\mathbf{F}_e = \nabla \mathbf{Y}^{-1} \mathbf{P}^{-1}$  is the *elastic deformation tensor* describing the passive elastic response of the tissue material to ensure its integrity.

For simplicity, we treat soft tissues as isotropic, compressible neo-Hookean elastic material. The strain energy is given by  $W(\mathbf{F}_e) = \frac{1}{2}\mu(\bar{I}_1 - d) + \frac{1}{2}K(J_e - 1)^2$ , where  $\mu$  and  $K$  are, respectively, the shear and bulk modulus. The integer  $d$  ( $= 2$  or  $3$ ) is the dimension of the tissue and  $\bar{I}_1 = J_e^{-2/d} \text{Tr}(\mathbf{F}_e^T \mathbf{F}_e)$  is the first invariant of the isochoric part of the *right Cauchy-Green deformation tensor*  $\mathbf{F}_e^T \mathbf{F}_e$ .  $J_e = \det(\mathbf{F}_e)$  is the volumetric (area) change due to pure elastic deformation in 3D (2D) tissue. By the stress-strain relation  $\boldsymbol{\sigma} = J_e^{-1} \frac{\partial W}{\partial \mathbf{F}_e} \mathbf{F}_e^T$ , we have

$$\boldsymbol{\sigma} = \mu J_e^{-\frac{2+d}{d}} \left( \mathbf{F}_e \mathbf{F}_e^T - \frac{I_1}{d} \mathbf{I} \right) + K(J_e - 1) \mathbf{I}, \quad (1)$$

for the elastic stress in  $d$ -dimension, where  $I_1 = \text{Tr}(\mathbf{F}_e^T \mathbf{F}_e)$ . The stress can be decomposed as  $\boldsymbol{\sigma} = \boldsymbol{\sigma}_s + \boldsymbol{\sigma}_p$  – the sum of the deviatoric part  $\boldsymbol{\sigma}_s$  (proportional to  $\mu$ ) and the isotropic part  $\boldsymbol{\sigma}_p$  (proportional to  $K$ ). For incompressible materials, i.e.,  $J_e \equiv 1$ , the isotropic part of the stress vanishes. Instead, a pressure term should be introduced (as a Lagrangian multiplier) for maintaining incompressibility [32, 33].

Mass conservation yields the evolution of tissue density

$$\dot{\rho} = \partial_t \rho + \mathbf{v} \cdot \nabla \rho = \rho(\gamma - \nabla \cdot \mathbf{v}), \quad (2)$$

where  $\rho(\mathbf{x}, t)$  is the tissue mass per unit volume,  $\mathbf{v}$  is the velocity, and  $\gamma(\mathbf{x}, t)$  is the rate of material production or loss (or rate of active growth). Assuming that the mass of tissue material within individual cells is roughly uniform (i.e., the rates of cell division and cell growth are strictly synchronized),  $\rho$  can be used to measure the cell (number) density relatively. In this case,  $\gamma(\mathbf{x}, t)$  is equivalent to the rate of cell number change due to cell proliferation and apoptosis, which is regulated by chemical and mechanical factors.

Since elastic deformation conserves mass, we have the relation  $J_e \rho = \rho_R$  at any given time  $t$ , where  $\rho_R$  is the stress-free tissue density. We assume that the local rate of volume or area constriction  $\gamma_c > 0$  can increase stress-free tissue density by  $\dot{\rho}_R = \gamma_c \rho_R$  (see *SI Appendix*). Taking these relations with Eq. 2, we can derive

$$\dot{J}_e = J_e(\nabla \cdot \mathbf{v} + \gamma_c - \gamma). \quad (3)$$

In 2D tissues, myosin-dependent contractility can result in  $\gamma_c > 0$ , which can effectively increase the  $J_e$ . Notice when  $J_e > 1$ , tissue is under tension, and when  $J_e < 1$ , tissue is under compression. If the tissue material is incompressible, we have  $\rho \equiv \rho_R \equiv \text{const.}$  and  $J_e \equiv 1$ . In this case,  $\dot{\rho} = 0$  from Eq. 2 leads to the condition for incompressible flow with source or sink  $\nabla \cdot \mathbf{v} = \gamma$ . In addition,  $\dot{J}_e = 0$  leads to zero local volumetric or area constriction  $\gamma_c = 0$ .

### Rearrangement

We describe the tissue rearrangement by introducing the rate of rearrangement  $\beta$ , which measures how fast the initial configuration of the tissue adapts to the current configuration:

$$\dot{\mathbf{y}} = \partial_t \mathbf{y} + \mathbf{v} \cdot \nabla \mathbf{y} = \beta(\mathbf{x} - \mathbf{y}). \quad (4)$$

In principle,  $\beta$  can vary spatiotemporally, regulated by oriented cell divisions that redistribute cell masses in the favor of relaxing stresses and cell-cell and cytoskeleton rearrangement without divisions. Here we consider it as spatially uniform for simplicity. This evolution equation can be rewritten as the dynamics of adaptive displacement  $\mathbf{u} = \mathbf{x} - \mathbf{y}$  with decaying rate  $\beta$ ,  $\dot{\mathbf{u}} = \mathbf{v} - \beta\mathbf{u}$ . When  $\beta = 0$ , we recover the classical connection between displacement and velocity  $\dot{\mathbf{u}} = \mathbf{v}$ . With this adaptive displacement, the new model is able to capture various behavior of previous linear viscoelastic models [25, 28] when the rate of tissue rearrangement is faster than the rate of differential growth and constriction, i.e.,  $\gamma/\beta \ll 1$  and  $\gamma_c/\beta \ll 1$  (see the discussion in *Multi-timescale Model Behavior*).

### Prestrain

For simplicity, we assume the accumulated prestrain tensor  $\mathbf{P} = J_p^{1/d}\mathbf{I}$  to be isotropic, where  $J_p = \det(\mathbf{P}) = \det(\nabla\mathbf{Y}^{-1})/J_e$ . From Eqs. 3 and 4 and denoting  $\Gamma = \gamma - \gamma_c$ , we can derive the evolution of  $J_p$

$$\dot{J}_p = J_p[\Gamma + \beta(d - \text{Tr}[\nabla\mathbf{Y}^{-1}])], \quad (5)$$

which describes the competition between active growth and constriction (reflected by  $\Gamma$ ) and rearrangement (reflected by the term proportional to  $\beta$ ) in the accumulation of prestrain (see *SI Appendix* for details).

At each time point, considering that the tissue mechanics is in an instantaneous mechanical equilibrium dominated by elastic stress, we have  $\nabla \cdot \boldsymbol{\sigma} = 0$ . Taking this together with Eq. 1 and the evolution equations Eqs. 2–5, we establish a coupled nonlinear system for describing the active tissue mechanics driven by the spatiotemporal patterns of growth  $\gamma$  and constriction  $\gamma_c$ , with proper initial and boundary conditions.

### MULTI-TIMESCALE MODEL BEHAVIOR

In the following, we will demonstrate the behavior of stress generation and relaxation in this new coupled system in its linearized regime.

#### Viscoelastic Tissue Mechanics in Short Timescale

By assuming that the rate of tissue growth and constriction is slower than the rate of tissue rearrangement, i.e.,  $\Gamma/\beta \sim O(\epsilon)$  and  $\epsilon \ll 1$ , the accumulated prestrain can be decomposed as  $J_p = J_0(1+g)$  where  $J_0$  is the initial global prestrain (i.e.,  $J_0 = \text{const.}$ ) and the differential prestrain  $g(\mathbf{x}, t) \sim O(\epsilon)$ . Considering the characteristic

time  $T \sim 1/\beta$ , we can derive the leading-order approximation of Eq. 5 as

$$\partial_t g = \Gamma - \beta \nabla \cdot \mathbf{u}, \quad (6)$$

where the advection term is dropped as the higher order term of  $\epsilon$ . By assuming  $|\mathbf{u}| \sim O(\epsilon)$  and  $|\nabla \mathbf{u}| \sim O(\epsilon)$  small, we can derive the leading-order linear approximation of Eq. 4 as

$$\partial_t \mathbf{u} = \mathbf{v} - \beta \mathbf{u} \quad (7)$$

where  $|\mathbf{v}| \sim O(\epsilon)$  and the advection term is, again, dropped as the higher order term of  $\epsilon$ .

Now, we can linearize the stress-strain relation Eq. 1, and decompose it into the isotropic part and the deviatoric part (see *SI Appendix* for details):

$$\boldsymbol{\sigma}_p = K(J_0^{-1} - 1)\mathbf{I} + KJ_0^{-1}(\nabla \cdot \mathbf{u} - g)\mathbf{I}, \quad (8)$$

$$\boldsymbol{\sigma}_s = \mu J_0(\nabla \mathbf{u} + \nabla \mathbf{u}^T - (2/d)(\nabla \cdot \mathbf{u})\mathbf{I}), \quad (9)$$

where the first term  $K(J_0^{-1} - 1)\mathbf{I}$  in  $\boldsymbol{\sigma}_p$  is the uniform stress due to the global prestrain  $J_0$ , and is not necessarily  $\sim O(\epsilon)$ . Differentiating  $\boldsymbol{\sigma}_p$  in time, the leading-order evolution of the isotropic stress (or the pressure) is given by

$$\partial_t \boldsymbol{\sigma}_p = \frac{K}{J_0}(\nabla \cdot \mathbf{v} - \Gamma)\mathbf{I}, \quad (10)$$

where the right-hand side reflects the competition between the rate of local volume expansion ( $\nabla \cdot \mathbf{v}$ ) and the rate of active growth and constriction ( $\Gamma = \gamma - \gamma_c$ ) on generating the isotropic stress with “effective” bulk modulus  $K/J_0$ . It indicates that the tissue can be stiffened in its bulk modulus when  $J_0 < 1$ , which can be associated with actomyosin-dependent contractility [36]. When only proliferation and apoptosis are considered (i.e.,  $\gamma_c = 0$ ), the dynamics of the isotropic stress is controlled by  $\gamma$ , which is consistent with the pressure dynamics description in [28]. However, an independent relaxation time of pressure is introduced in their formulation to describe the tissue mechanics close to homeostasis. We will soon show that in our model, the dissipation of the deviatoric stress and local force balance together result in the dissipation of pressure, which means that the rate of rearrangement sets both the relaxation time of the pressure and the deviatoric stress.

Differentiating the deviatoric stress Eq. 9 in time and using Eq. 7, we obtain the Maxwell model of viscoelastic materials

$$\boldsymbol{\sigma}_s + \frac{1}{\beta} \partial_t \boldsymbol{\sigma}_s = \frac{\mu J_0}{\beta} \left( \nabla \mathbf{v} + \nabla \mathbf{v}^T - \frac{2}{d}(\nabla \cdot \mathbf{v})\mathbf{I} \right), \quad (11)$$

where  $(\nabla \mathbf{v} + \nabla \mathbf{v}^T)$  defines the strain rate,  $\beta$  serves as the rate of stress relaxation and the ratio  $\mu J_0/\beta$  plays the role of “effective” viscosity. Note that in Eqs. 10 and

11 we use the time derivative  $\partial_t \boldsymbol{\sigma}$  in the linear approximation. In the general case of large deformation, the upper-convected time derivative  $\overset{\nabla}{\dot{\boldsymbol{\sigma}}} = \dot{\boldsymbol{\sigma}} - (\nabla \mathbf{v})^T \cdot \boldsymbol{\sigma} - \boldsymbol{\sigma} \cdot (\nabla \mathbf{v})$  should be applied. The Maxwell-like relaxation of deviatoric stress Eq. 11 reflects the fluidization of tissue by rearrangement, and hence we can use the rate of relaxation  $\beta$  to describe the fluidity of tissue. The tissue fluidization was also found by linear viscoelastic model with the stress relaxation timescale coupled with the orientated cell division and death [28]. However, in general, the tissue rearrangement is not necessarily coupled with cell division but can be also facilitated by cell-cell topological transition and the reorganization of the cytoskeletal elements. We have shown that the linear Maxwellian viscoelastic behavior is a special case of our model when the tissue rearrangement is faster than the active growth and constriction. In this case, both the rate of tissue rearrangement  $\beta$  and the global prestrain  $J_0$  can modulate tissue viscosity.

### Viscous Tissue Flow in Long Timescale

If we assume the characteristic time  $T \sim 1/\Gamma \gg 1/\beta$ , we have the quasi-steady-state relations from the leading order of Eqs. 6, 7 and 11, i.e.,  $\mathbf{v} = \beta \mathbf{u}$ ,  $\beta \nabla \cdot \mathbf{u} = \Gamma$  and  $\boldsymbol{\sigma}_s = \frac{\mu J_0}{\beta} \left( \nabla \mathbf{v} + \nabla \mathbf{v}^T - \frac{2}{d} (\nabla \cdot \mathbf{v}) \mathbf{I} \right)$ . Together with Eq. 8 and assuming  $\nabla \cdot \boldsymbol{\sigma} = 0$ , we can derive the tissue behavior as viscous fluid

$$\frac{\mu J_0}{\beta} \nabla^2 \mathbf{v} = \frac{K}{J_0} \nabla \left( g - \frac{\Gamma}{\beta} \right) - \frac{\mu J_0}{\beta} \left( 1 - \frac{2}{d} \right) \nabla \Gamma, \quad (12)$$

with the constraint

$$\nabla \cdot \mathbf{v} = \Gamma. \quad (13)$$

In 2D, the last term on the right-hand side of Eq. 12 vanishes, and our model is similar with the viscoelastic fluid model [25], where the viscous tissue flow is driven by the force generated by the gradient of myosin-dependent constriction. However, in our linearized fluid system, the rate of force-generating activities  $\Gamma$  is the driver of the tissue dynamics, which results in a field of accumulated differential prestrain  $g$  and tissue flow  $\mathbf{v}$ . The tissue mechanics and flow can be modulated by the rearrangement rate  $\beta$ , together with the effective bulk modulus  $K/J_0$  and viscosity  $\mu J_0/\beta$  that are regulated by the global prestrain  $J_0$ . The extent of tissue compression or extension can be computed as  $J_e = J_0^{-1} (1 + \Gamma/\beta - g) \neq 1$ . When  $\gamma_c = 0$ , we can derive an interesting behavior of the tissue such that it appears as incompressible flow due to  $\nabla \cdot \mathbf{v} = \gamma$  but can be under elastic compression or extension due to  $J_e = J_0^{-1} (1 + \gamma/\beta - g)$ .

### Mechanical Equilibrium in a 2D Disc

Considering a radially symmetric tissue disc with  $\Gamma$  being neither always positive nor always negative within the tissue, there exists an equilibrium tissue size  $R_{eq}$  such that

$$G(R_{eq}) = 0, \quad \text{where} \quad G(r) = \int_0^r \Gamma(r') r' dr'. \quad (14)$$

We can obtain the solutions in mechanical equilibrium from Eqs. 12 and 13 with the boundary condition  $\sigma_{rr}(R_{eq}) = K(J_0^{-1} - 1)$  (see *SI Appendix* for the linear model):

$$v = \frac{G(r)}{r} \quad \text{and} \quad g = \left( 1 + \frac{\mu J_0^2}{K} \right) \frac{\Gamma(r)}{\beta}. \quad (15)$$

Then, we can reconstruct the stresses and the area variation due to elastic deformation  $J_e$ :

$$\begin{aligned} \sigma_{rr} &= K(J_0^{-1} - 1) - \frac{2\mu J_0 G(r)}{\beta r^2}, \\ \sigma_{\theta\theta} &= K(J_0^{-1} - 1) + \frac{2\mu J_0}{\beta} \left( \frac{G(r)}{r^2} - \Gamma(r) \right), \\ J_e &= J_0^{-1} \left( 1 - \frac{\mu J_0^2}{K} \frac{\Gamma(r)}{\beta} \right). \end{aligned} \quad (16)$$

The stress has a uniform component induced by  $J_0$  and a spatial variation driven by differential growth and constriction  $\Gamma(r) = \gamma(r) - \gamma_c(r)$  and modulated by the effective viscosity  $\mu J_0/\beta$ . Interestingly, the variation of stress is independent on the bulk modulus  $K$ . Notice that the spatial variation of isotropic stress (pressure)  $\sim (\sigma_{rr} + \sigma_{\theta\theta})$  is also dissipated with large  $\beta/\mu J_0$ , suggesting it has the same relaxation time as deviatoric stress close to homeostasis. This behavior is very different from the pressure relaxation dynamics in [28].

The cell density ( $\rho = \rho_R/J_e$ ) can only reach equilibrium when  $\gamma_c = 0$  (otherwise  $\dot{\rho}_R = \gamma_c \rho R \dot{J}_e < 0$ ). When  $\gamma_c = 0$  (e.g., due to mechanical feedback mechanisms [37]), we have the distribution of cell density  $\rho = \rho_R J_0 (1 + \frac{\mu J_0^2}{K} \frac{\gamma(r)}{\beta})$  at equilibrium. Thus, the spatial variation in cell density is modulated by  $(K/J_0)/(\mu J_0)$ , the relative tissue compressibility and  $\beta/\gamma$ , the tissue fluidity relative to growth. Both large compressibility modulus and fluidity indicate small variation in cell density.

### NONLINEAR SIMULATIONS

We now perform numerical simulations with the nonlinear model for 2D radially symmetric tissue to investigate the regulation of the mechanical stress and cell density by tissue elasticity and fluidity in the nonlinear regime (see *SI Appendix* for the reduced radially symmetric nonlinear model). For simplicity, we assume that

there is no initial prestrain or elastic deformation, i.e.,  $u(r, 0) = 0$  and  $J_p(r, 0) = 1$ , and free boundary condition,  $\sigma_{rr}(R(t), t) = 0$ , where  $R(t)$  represents the boundary of the tissue disc and evolves as  $\dot{R}(t) = v(R, t)$  in the radial direction. Further, we assume that  $\gamma_c = 0$ , and therefore we have  $\rho_R = \text{const.} \equiv 1$  and  $\Gamma = \gamma$  is the growth rate. From now on, we set  $\mu = 1$  without loss of generality, and then  $K$  stands for the relative tissue compressibility modulus  $K/\mu$ .

### Regulation of Mechanical Stress and Cell Density

First, we assume  $K = 2$ ,  $\beta = 1$  (to set the characteristic timescale  $T \sim 1$ ), and that the growth is slower than the rearrangement ( $\Gamma/\beta$  is small), e.g.,  $\Gamma(r) = 0.1(1 - r)$  (shown in Fig. 2 B), to validate the findings from the linear analytical solutions. This choice of  $\Gamma$  gives the equilibrium tissue size of  $R_{eq} = 1.5$  from Eq. 14. We simulate the growth of the tissue from a smaller size  $R = 1.45$  until it reaches its mechanical equilibrium state. See the dynamics during the tissue growth in Fig. S1. At equilibrium, the results of the stresses (Fig. 1 A and B) and the inverse of (normalized) cell density  $J_e = (\rho/\rho_R)^{-1}$  (Fig. 1 C) from nonlinear simulations matches well with the linear solutions. Due to the negative gradient of  $\Gamma$ , the tissue is under compression near the center (where the

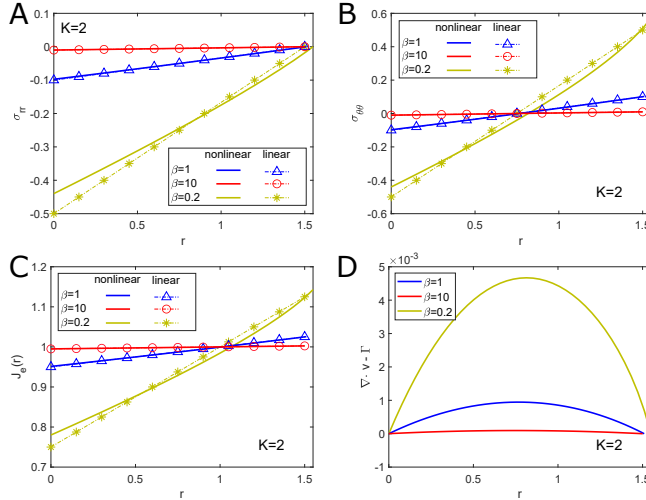


FIG. 1. Effect of tissue rearrangement on the mechanical state of tissue at equilibrium. (A and B) Radial and circumferential stresses. (C) The inverse of cell density  $J_e = \rho_R/\rho$ . Cells are compressed and concentrated near the center and stretched near the boundary. The nonlinear solutions (solid lines) agrees with the linear solutions (dashed lines with markers) when the tissue rearrangement is much faster than tissue growth ( $\beta = 1, 10$ ). For slower rearrangement ( $\beta = 0.2$ ), the nonlinear solutions start to deviate from linear solutions. (D) Compressibility of tissue flow. For incompressible flow,  $\nabla \cdot v - \Gamma = 0$  (when  $\gamma_c = 0$ ). See text for more details.

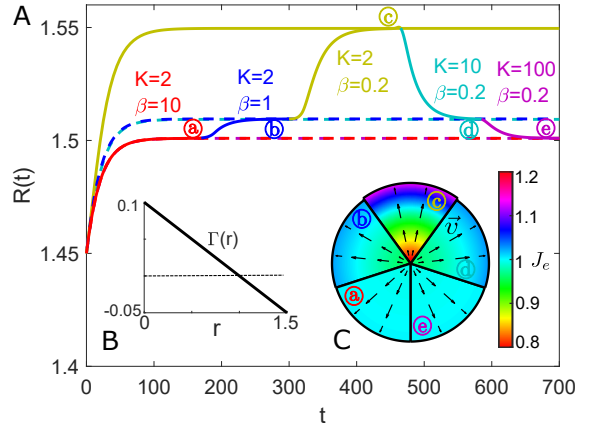


FIG. 2. (A) Evolution of tissue size with dynamical modulation of  $\beta$  and  $K$ . The solid line shows the evolution with dynamical modulation and the dashed lines show the evolution without modulation. a-e indicate the equilibrium states for each set of parameters  $\beta$  and  $K$ . (B) The spatial profile of growth rate  $\Gamma = 0.1(1 - r)$ , where  $\Gamma > 0$  (above dashed line) induces growth and  $\Gamma < 0$  (below dashed line) induces death. (C) The distributions of the inverse of cell density  $J_e$  and the tissue flow velocity  $v$ , at equilibria a-e in (A). The color map shows the values of  $J_e$ . The arrows indicate the direction and dimensionless magnitude of the tissue velocity.

density is larger) and under extension near the boundary (where the density is smaller), and tissue flows from the center to the boundary (Fig. 2 C). We further increase  $\beta = 10$  and find that the stresses are dissipated and the density is uniform, which is also in a good agreement with the linear solutions. When the rearrangement is slower ( $\beta = 0.2$ ), the variations in stresses and the cell density become more obvious, and the nonlinear solution starts to deviate quantitatively from the linear solution. For  $\beta = 0.2, 1, 10$ , the tissue flow becomes more incompressible as  $\beta$  increases (Fig. 1 D).

If we increase the tissue compressibility modulus  $K$ , the tissue becomes more incompressible and hence undergoes more incompressible flow. As  $K$  increases, the distribution of cell density becomes more uniform. However, the stress distribution is scarcely altered as  $K$  increases (Fig. S2). These behaviors of cell density and stresses are qualitatively consistent with the linear solution in Eq. 16.

We find that the equilibrium size of the tissue depends on  $\beta$  and  $K$ , but not on the initial size (Fig. S3). Moreover, if we modulate dynamical  $\beta$  and  $K$  after the tissue reaches an equilibrium state, the dynamics of the tissue size resumes and results in a new steady state (Fig. 2 A). When  $\beta$  or  $K$  is large, the equilibrium size is close to  $R_{eq} = 1.5$  determined by our choice of  $\Gamma$  and Eq. 14; however, when  $\beta$  and  $K$  are both small, the tissue size reaches a different equilibrium state, which is a consequence of nonlinear effects and will be discussed below.

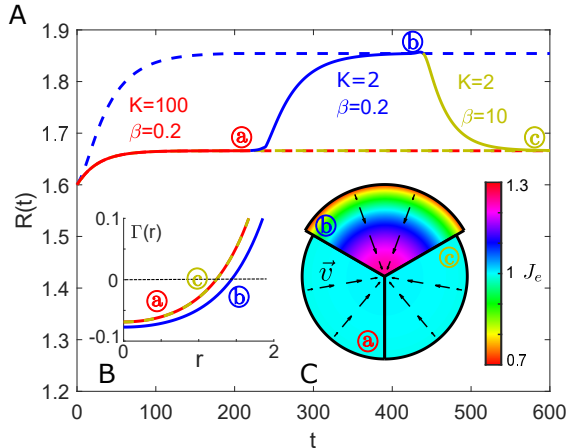


FIG. 3. (A) Evolution of tissue size with dynamical modulation of  $\beta$  and  $K$ . The solid (dashed) line shows the evolution with (without) dynamical modulation. a-c indicate the equilibria for each set of parameters  $\beta$  and  $K$ . (B) The spatial profile of  $\Gamma$ , coupled with the reaction-diffusion process of growth factor (with  $L = 0.5$ ,  $\lambda_p = 0.2$  and  $\lambda_a = 0.1$ ). The dashed line indicates the level of  $\Gamma = 0$ . The profiles of  $\Gamma$  for the equilibrium a and c are identical due to the same equilibrium tissue size  $R(t)$ . (C) The distributions of the inverse of cell density  $J_e$  and the tissue flow velocity  $v$ , at equilibria a-c in (A). The color map shows the values of  $J_e$ . The arrows indicate the direction and dimensionless magnitude of the tissue velocity.

#### Nonlinear Effect on Tissue Size

When the tissue is in mechanical equilibrium,  $J_e$  does not change locally within the tissue, i.e.,  $\partial_t J_e = J_e(\nabla \cdot \mathbf{v} - \Gamma) - \mathbf{v} \cdot \nabla J_e = 0$ . Integrating the equation (divided by  $J_e$ ) in a 2D disc, we obtain the coupling between the growth rate and the (nonlinear) advection in tissue flow, which provides a condition for the equilibrium size  $R_{eq}$

$$\int_0^{R_{eq}} \Gamma r dr = - \int_0^{R_{eq}} \frac{1}{J_e} \left( v \frac{\partial J_e}{\partial r} \right) r dr. \quad (17)$$

When the tissue is incompressible or highly fluidized ( $K = 100$  or  $\beta = 10$ ),  $J_e$  is (almost) uniform constant,  $\partial_r J_e = 0$ , and hence  $R_{eq}$  is solely determined by the growth pattern  $\Gamma$  via the integrated growth rate condition  $G(R_{eq}) = 0$  as in the linear case by Eq. 14. However, when the tissue is highly compressible or weakly fluidized (i.e.,  $K$  and  $\beta$  are small), the equilibrium size is altered by the nonlinear advection term in tissue flow  $v \partial_r J_e \neq 0$  as predicted by Eq. 17. The modulation of tissue size by material properties is a nonlinear effect for compressible tissue that has not been predicted by previous models.

#### Growth Rate Coupled with Chemical Signals

We further investigate whether the above behaviors persist when  $\Gamma$  is no longer described as an *a priori* function and is coupled with a field of growth factor or nutrient that follows the reaction-diffusion process. In the 2D disc, we assume that the concentration of the growth factor is constant at the boundary, i.e.,  $c(R(t), t) = 1$ , and diffuses to the central region by

$$\frac{1}{\lambda} \frac{\partial c}{\partial t} = L^2 \frac{1}{r} \frac{\partial}{\partial r} \left( r \frac{\partial c}{\partial r} \right) - c, \quad \text{for } 0 < r < R(t), \quad (18)$$

with no flux boundary condition at the center  $\partial_r c(0, t) = 0$ . The turnover rate of the growth factor  $\lambda$  determines the characteristic time of the reaction-diffusion process and  $L = \sqrt{D/\lambda}$  is the diffusion length. Assuming  $\lambda \gg \Gamma$ , we can solve  $c$  by the quasi-steady-state approximation of Eq. 18 for tissue radius  $R(t)$  at each time point. In general,  $c$  decreases from the boundary to the center of the tissue, and the local concentration  $c$  further decreases as  $R(t)$  increases (see Fig. S4 for details).

We consider that the local rate of active growth is coupled with the concentration  $c$  in the simplified form of

$$\Gamma = c \lambda_p - \lambda_a, \quad (19)$$

where  $c \lambda_p$  and  $\lambda_a$  are the local rates of cell proliferation and apoptosis, respectively. The resultant distribution of growth rate  $\Gamma$  has a positive gradient as  $r$  increases (Fig. 3 B), which induces the inward tissue flow at equilibrium (see Fig. 3 C for  $v$  at equilibrium and Fig. S4 for the dynamics before equilibrium). The cell density displays a positive gradient such that the cells are under tension in the center and compression near the boundary, which accentuates as  $K$  and  $\beta$  decrease (see Fig. 3 C for  $J_e$ ). Similar as the case where  $\Gamma$  is given *a priori* (Fig. 2), the equilibrium tissue size can be modulated by the change of  $K$  and  $\beta$  (shown in Fig. 3 A) due to the same mechanism as explained in *Nonlinear Effect on Tissue Size*. However, the amplitude of the variation in tissue size is significantly larger due to the stronger nonlinear effect induced by the coupling with the reaction-diffusion process of the growth factor. Moreover, we find that stress distribution is sensitive to the change of  $K$ , where decreasing compressibility modulus  $K$  increases stress heterogeneity (see Fig. S5).

#### Integrating Chemomechanical Growth Signals

As there is growing evidence that tissue growth responds to mechanical cues [1–10, 18–20], we ask how tissue mechanics nonlinearity influences tissue size via mechanical feedback mechanisms. While it is still an open question how the mechanical and chemical signals are integrated in the execution of tissue growth, especially

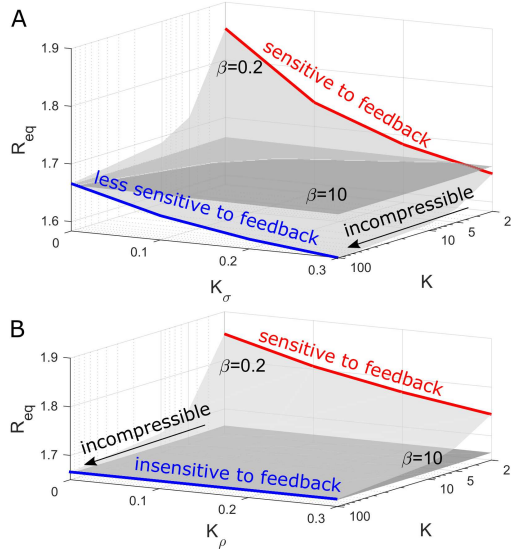


FIG. 4. Tissue size at equilibrium modulated by material properties ( $K$  and  $\beta$ ) and feedback intensities ( $K_\sigma$  and  $K_\rho$ ). (A) Tissue size at equilibrium  $R_{eq}$  with stress-sensing feedback only, as a function of  $K$  and  $K_\sigma$  for different values of  $\beta$ . (B) Tissue size at equilibrium  $R_{eq}$  with density-sensing feedback only, as a function of  $K$  and  $K_\rho$  for different values of  $\beta$ .

with differential growth [37], we consider that the local proliferation rate being modulated by local stresses and cell density with feedback intensities  $K_\sigma$  ( $\geq 0$ ) and  $K_\rho$  ( $\geq 0$ ), respectively, on top of the dependence on local growth factor concentration  $c$ :

$$\Gamma = \frac{c\lambda_p}{1 - K_\sigma(\sigma_{rr} + \sigma_{\theta\theta}) + K_\rho(\rho - 1)} - \lambda_a. \quad (20)$$

In the nonlinear regime where tissue is moderately compressible ( $K = 2$ ) and fluidized ( $\beta = 0.2$ ), both the increases in the feedback intensities  $K_\sigma$  and  $K_\rho$  decrease the tissue size in equilibrium (Fig. 4). Moreover, the increase in  $K_\sigma$  or  $K_\rho$  reduces the spatial heterogeneity of stresses or the cell density, respectively (Fig. S6). However, when the tissue becomes more incompressible (increasing  $K$ ) or more fluidic (increasing  $\beta$ ), the sensitivity of the tissue size variation to the change of feedback strengths decreases. In particular, when the tissue is nearly incompressible ( $K = 100$ ), the density-sensing feedback no longer affects the tissue size since the density is uniform. When the tissue highly fluidized ( $\beta = 10$ ), the stresses are dissipated and cell density is uniform, and hence both the stress-sensing and density-sensing feedback mechanisms become ineffective (Fig. 4). In conclusion, the nonlinear effects in tissue mechanics, associated with lower level of fluidity and incompressibility, can increase the sensitivity of tissue size variation to mechanical feedback machineries.

## DISCUSSION

In this paper, we have developed a nonlinear elastic model which couples the dynamics of force-generating activities (rate defined as  $\Gamma$ ) and force-dissipating activities (rate defined as  $\beta$ ) with active tissue mechanics. The force-generating activities include cell proliferation, apoptosis, and myosin-dependent contractility and the the force-dissipating activities include the cell-cell rearrangement [11, 12] and cytoskeleton reorganization [21]. Only when force-dissipating activities are much faster than force-generating activities ( $\Gamma/\beta \ll 1$ ), this nonlinear model can be reduced to a linear viscoelastic model at the timescale of force-dissipating activities ( $T \sim 1/\beta$ ), which is similar to previous Maxwell-type viscoelastic models [28–30]. However, in these models, it is assumed that the two timescales are synchronized. At the timescale of force-generating activities, our model is reduced to an active viscous fluid model, which is similar to previous models [24, 25]. In ref. [24], an active viscous fluid model has been used to explain the epithelial tissue flow in dorsal thorax of pupal-stage *Drosophila*, in which the force is generated by the gradient of atypical myosin Dachs and drives the effective viscous tissue flow. However, why tissues can exhibit fluidic behaviors, especially under significant evolving elastic strains [26], has not been explained. Our model explains this conundrum as a limit case between the two-timescale competition. In the limit of  $\Gamma/\beta \ll 1$ , we have found the effective tissue viscosity  $\mu J_0/\beta$ , determined not only by the shear modulus of the tissue  $\mu$  and the rearrangement rate  $\beta$ , but also by the level of global prestrain. In ref. [25], an active viscous fluid model is used to fit the epithelial tissue flow during gastrulation and has suggested the global viscosity to be time-dependent. In particular, they found that the ratio between the shear viscosity and the bulk viscosity decreases in time. We suggest that this decreased ratio may be explained by the decreased prestrain  $J_0 (< 1)$  due to a globally enhanced myosin II-dependent tissue constriction on top of the spatial gradient. This is the case in dorsal thorax, where the global prestrain  $J_0$  is suggested to further decrease in time due to the global elevation of myosin II-dependent constriction [27].

We have demonstrated how strains and stresses are developed in the competition between tissue growth and rearrangement. We have shown that tissue mechanics can be accurately described by the linear model when  $\Gamma/\beta \ll 1$ , and increasing the ratio of two timescales  $\Gamma/\beta$  results in more heterogeneous strains and stresses. As the two timescales are comparable (i.e.,  $\beta \sim \Gamma$ ), the nonlinear effects in the tissue mechanics become considerable. Interestingly, when  $\beta \sim \Gamma$ , we have found the change of tissue elastic property  $K/\mu$  can regulate the size of a circular tissue, which is a nonlinear effect due to advection in tissue flow. These nonlinear effects on the

tissue size and mechanics become significant when the growth rate is coupled with the local concentration of a growth factor or nutrient, patterned by a spatiotemporal reaction-diffusion process in the growing tissue. By coupling  $\Gamma$  with mechanical cues, we have demonstrated that the tissue elastic properties  $K/\mu$  and the rate of rearrangement  $\beta$  can further modulate tissue size and mechanics with mechanical feedbacks. Given the details of how growing tissues sense [4, 38, 39] and integrate [5, 12, 37, 40] mechanical signals are still under investigation, we have assumed a simple function where the local growth rate  $\Gamma$  responds to both local stresses and cell density via two feedback intensities  $K_\sigma$  and  $K_\rho$ , respectively. While increasing either  $K_\sigma$  or  $K_\rho$  reduces the tissue size and stress-and-strain heterogeneity in equilibrium, we have found that the tissue size variation is more sensitive to these feedback intensities when tissue is less fluidic and more compressible (expandable) which is exactly when nonlinear effects are more pronounced. This finding suggests another layer of complexity in the tissue size control from the dynamics of stress and strain generation and relaxation.

Traditional nonlinear elastic growth theory has been used to understand growth and shape formations [31, 32]. For example, it explains the formations of gut lumen ridges [41, 42] and mammalian cortex folds [43] as elastic deformation due to the accumulated stresses induced by differential growth. In most previous works in which this theory is applied, there is a lack of description of tissue dynamics, especially the connection between tissue mechanics and cell activities that generate or dissipate stress and strain. Thus, tissue rearrangement and mechanical feedback in the shape formation of growing tissues have not been explored. Our model is ideal for studying their roles in shape formations. Our next step is to investigate the role of tissue rearrangement and mechanical feedbacks in regulating the emergence of border undulation and out-of-plane tissue deformation of the circular tissue disc. Further, we will use this model to simulate active tissue mechanics in a general 2D and 3D tissue domain, such as large-scale tissue morphogenesis [22–24].

## ACKNOWLEDGMENT

M.W acknowledges funding from NSF-DMS-2012330.

---

- [1] Jean-Paul Vincent, Alexander G Fletcher, and L Alberto Baena-Lopez. Mechanisms and mechanics of cell competition in epithelia. *Nature reviews Molecular cell biology*, 14(9):581–591, 2013.
- [2] Cristina Clavería and Miguel Torres. Cell competition: mechanisms and physiological roles. *Annual review of cell and developmental biology*, 32:411–439, 2016.

- [3] Nicholas E Baker. Emerging mechanisms of cell competition. *Nature Reviews Genetics*, 21(11):683–697, 2020.
- [4] Jin-Hong Kim, Keiichiro Kushiro, Nicholas A. Graham, and Anand R. Asthagiri. Tunable interplay between epidermal growth factor and cell–cell contact governs the spatial dynamics of epithelial growth. *Proceedings of the National Academy of Sciences USA*, 106(27):11149–11153, 2009.
- [5] Nam-Gyun Kim, Eunjin Koh, Xiao Chen, and Barry M Gumbiner. E-cadherin mediates contact inhibition of proliferation through hippo signaling-pathway components. *Proceedings of the National Academy of Sciences USA*, 108(29):11930–11935, 2011.
- [6] Mariana Pavel, Maurizio Renna, So Jung Park, Fiona M Menzies, Thomas Ricketts, Jens Füllgrabe, Avraham Ashkenazi, Rebecca A Frake, Alejandro Carnicer Lombarte, Carla F Bento, et al. Contact inhibition controls cell survival and proliferation via yap/taz-autophagy axis. *Nature communications*, 9(1):1–18, 2018.
- [7] Boris I. Shraiman. Mechanical feedback as a possible regulator of tissue growth. *Proceedings of the National Academy of Sciences USA*, 102(9):3318–3323, 2005.
- [8] Tinri Aegeerter-Wilmsen, Christof M. Aegeerter, Ernst Hafen, and Konrad Basler. Model for the regulation of size in the wing imaginal disc of *Drosophila*. *Mechanisms of Development*, 124(4):318–326, 2007.
- [9] Lars Hufnagel, Aurelio A. Teleman, Hervé Rouault, Stephen M. Cohen, and Boris I. Shraiman. On the mechanism of wing size determination in fly development. *Proceedings of the National Academy of Sciences USA*, 104(10):3835–3840, 2007.
- [10] Yuanwang Pan, Idse Heemskerk, Consuelo Ibar, Boris I. Shraiman, and Kenneth D. Irvine. Differential growth triggers mechanical feedback that elevates Hippo signaling. *Proceedings of the National Academy of Sciences USA*, 113(45):E6974–E6983, 2016.
- [11] Thomas Lecuit, Pierre-François Lenne, and Edwin Munro. Force generation, transmission, and integration during cell and tissue morphogenesis. *Annual review of cell and developmental biology*, 27(1):157–184, 2011.
- [12] Loïc LeGoff and Thomas Lecuit. Mechanical forces and growth in animal tissues. *Cold Spring Harbor perspectives in biology*, 8(3):a019232, 2016.
- [13] Carl-Philip Heisenberg and Yohanns Bellaléche. Forces in tissue morphogenesis and patterning. *Cell*, 153(5):948–962, 2013.
- [14] Duoja Pan. The hippo signaling pathway in development and cancer. *Developmental cell*, 19(4):491–505, 2010.
- [15] Bin Zhao, Li Li, Qunying Lei, and Kun-Liang Guan. The hippo–yap pathway in organ size control and tumorigenesis: an updated version. *Genes & development*, 24(9):862–874, 2010.
- [16] Fa-Xing Yu, Bin Zhao, and Kun-Liang Guan. Hippo pathway in organ size control, tissue homeostasis, and cancer. *Cell*, 163(4):811–828, 2015.
- [17] Yonggang Zheng and Duoja Pan. The hippo signaling pathway in development and disease. *Developmental cell*, 50(3):264–282, 2019.
- [18] Gabriel Helmlinger, Paolo A Netti, Hera C Lichtenbeld, Robert J Melder, and Rakesh K Jain. Solid stress inhibits the growth of multicellular tumor spheroids. *Nature biotechnology*, 15(8):778, 1997.
- [19] Fabien Montel, Morgan Delarue, Jens Elgeti, Laurent Malaquin, Markus Basan, Thomas Risler, Bernard Ca-

bane, Danijela Vignjevic, Jacques Prost, Giovanni Capello, et al. Stress clamp experiments on multicellular tumor spheroids. *Physical review letters*, 107(18):188102, 2011.

[20] Morgan Delarue, Fabien Montel, Danijela Vignjevic, Jacques Prost, Jean François Joanny, and Giovanni Capello. Compressive stress inhibits proliferation in tumor spheroids through a volume limitation. *Biophysical Journal*, 107(8):1821–1828, 2014.

[21] Konstantin Doubrovinski, Michael Swan, Oleg Polyakov, and Eric F Wieschaus. Measurement of cortical elasticity in *drosophila melanogaster* embryos using ferrofluids. *Proceedings of the National Academy of Sciences USA*, 114(5):1051–1056, 2017.

[22] Matteo Rauzi, Pierre-François Lenne, and Thomas Lecuit. Planar polarized actomyosin contractile flows control epithelial junction remodelling. *Nature*, 468(7327):1110–1114, 2010.

[23] Boris Guirao, Stéphane U Rigaud, Floris Bosveld, Anaïs Bailles, Jesús López-Gay, Shuji Ishihara, Kaoru Sugimura, François Graner, and Yohanns Bellaïche. Unified quantitative characterization of epithelial tissue development. *eLife*, 4:e08519, dec 2015.

[24] Floris Bosveld, Isabelle Bonnet, Boris Guirao, Sham Tlili, Zhimin Wang, Ambre Petitalot, Raphaël Marichand, Pierre-Luc Bardet, Philippe Marcq, François Graner, et al. Mechanical control of morphogenesis by fat/dachsous/four-jointed planar cell polarity pathway. *Science*, 336(6082):724–727, 2012.

[25] Sebastian J Streichan, Matthew F Lefebvre, Nicholas Noll, Eric F Wieschaus, and Boris I Shraiman. Global morphogenetic flow is accurately predicted by the spatial distribution of myosin motors. *eLife*, 7:e27454, feb 2018.

[26] Isabelle Bonnet, Philippe Marcq, Floris Bosveld, Luc Fetler, Yohanns Bellaïche, and François Graner. Mechanical state, material properties and continuous description of an epithelial tissue. *Journal of The Royal Society Interface*, 9(75):2614–2623, 2012.

[27] Scott Curran, Charlotte Strandkvist, Jasper Bathmann, Marc de Gennes, Alexandre Kabla, Guillaume Salbreux, and Buzz Baum. Myosin ii controls junction fluctuations to guide epithelial tissue ordering. *Developmental cell*, 43(4):480–492, 2017.

[28] Jonas Ranft, Markus Basan, Jens Elgeti, Jean-François Joanny, Jacques Prost, and Frank Jülicher. Fluidization of tissues by cell division and apoptosis. *Proceedings of the National Academy of Sciences USA*, 107(49):20863–20868, 2010.

[29] Ojan Khatib Damavandi and David K. Lubensky. Statistics of noisy growth with mechanical feedback in elastic tissues. *Proceedings of the National Academy of Sciences USA*, 116(12):5350–5355, 2019.

[30] Antoine Fruleux and Arezki Boudaoud. Modulation of tissue growth heterogeneity by responses to mechanical stress. *Proceedings of the National Academy of Sciences USA*, 116(6):1940–1945, 2019.

[31] Edward K. Rodriguez, Anne Hoger, and Andrew D. McCulloch. Stress-dependent finite growth in soft elastic tissues. *Journal of Biomechanics*, 27(4):455–467, 1994.

[32] Davide Ambrosi, Martine Ben Amar, Christian J. Cyron, Antonio DeSimone, Alain Goriely, Jay D. Humphrey, and Ellen Kuhl. Growth and remodelling of living tissues: Perspectives, challenges and opportunities. *Journal of the Royal Society Interface*, 16(157), 2019.

[33] H. Yan, D. Ramirez-Guerrero, J. Lowengrub, and M. Wu. Stress generation, relaxation and size control in confined tumor growth. *bioRxiv*, 2019.

[34] Georges-Henri Cottet, Emmanuel Maitre, and Thomas Milcent. Eulerian formulation and level set models for incompressible fluid-structure interaction. *ESAIM: Mathematical Modelling and Numerical Analysis*, 42(3):471–492, may 2008.

[35] Ken Kamrin, Chris H. Rycroft, and Jean Christophe Nave. Reference map technique for finite-strain elasticity and fluid-solid interaction. *Journal of the Mechanics and Physics of Solids*, 60(11):1952–1969, nov 2012.

[36] Natalie C. Heer and Adam C. Martin. Tension, contraction and tissue morphogenesis. *Development*, 144(23):4249–4260, dec 2017.

[37] Kenneth D. Irvine and Boris I. Shraiman. Mechanical control of growth: Ideas, facts and challenges. *Development (Cambridge)*, 144(23):4238–4248, 2017.

[38] Cordelia Rauskolb, Shuguo Sun, Gongping Sun, Yuan-wang Pan, and Kenneth D Irvine. Cytoskeletal tension inhibits hippo signaling through an ajuba-warts complex. *Cell*, 158(1):143–156, 2014.

[39] Alberto Elosegui-Artola, Ion Andreu, Amy EM Beedle, Ainhoa Lezamiz, Marina Uroz, Anita J Kosmalska, Roger Oria, Jenny Z Kechagia, Palma Rico-Lastres, Anabel-Lise Le Roux, et al. Force triggers yap nuclear entry by regulating transport across nuclear pores. *Cell*, 171(6):1397–1410, 2017.

[40] Luis Alberto Baena-Lopez, Hisashi Nojima, and Jean-Paul Vincent. Integration of morphogen signalling within the growth regulatory network. *Current opinion in cell biology*, 24(2):166–172, 2012.

[41] Amy E Shyer, Tuomas Tallinen, Nandan L Nerurkar, Zhiyan Wei, Eun Seok Gil, David L Kaplan, Clifford J Tabin, and L Mahadevan. Villification: how the gut gets its villi. *Science*, 342(6155):212–218, 2013.

[42] Martine Ben Amar and Fei Jia. Anisotropic growth shapes intestinal tissues during embryogenesis. *Proceedings of the National Academy of Sciences USA*, 110(26):10525–10530, 2013.

[43] Tuomas Tallinen, Jun Young Chung, François Rousseau, Nadine Girard, Julien Lefèvre, and Lakshminarayanan Mahadevan. On the growth and form of cortical convolutions. *Nature Physics*, 12(6):588–593, 2016.

**Supplementary Material for  
Nonlinear modeling reveals multi-timescale and higher-order effects in active tissue  
mechanics**

Chaozhen Wei<sup>1,\*</sup> and Min Wu<sup>1,2,†</sup>

<sup>1</sup>*Department of Mathematical Sciences, Worcester Polytechnic Institute, Worcester, MA 10605 USA*

<sup>2</sup>*Bioinformatics and Computational Biology, Worcester Polytechnic Institute, Worcester, MA 10605 USA*

(Dated: March 18, 2021)

**DERIVATION OF EVOLUTION OF TOTAL VOLUMETRIC CHANGE**

We starts from the evolution of adaptive reference map  $\mathbf{y} = \mathbf{Y}(\mathbf{x}, t)$  that relates the reference configuration  $\mathbf{y}$  and the current configuration  $\mathbf{x}$  in Eulerian coordinates

$$\frac{d\mathbf{y}}{dt} = \frac{\partial \mathbf{y}}{\partial t} + \mathbf{v} \cdot \nabla \mathbf{y} = \beta(\mathbf{x} - \mathbf{y}). \quad (1)$$

Notice that the geometric deformation tensor is  $\mathbf{F} = \nabla \mathbf{Y}^{-1}$  and the total volumetric change is  $J = \det(\nabla \mathbf{Y}^{-1})$ . Taking the gradient operator  $\nabla$  on the both sides of Eq. (1), we obtain the evolution of  $\nabla \mathbf{Y}$

$$\frac{\partial(\nabla \mathbf{Y})}{\partial t} + \mathbf{v} \cdot \nabla(\nabla \mathbf{Y}) = -\nabla \mathbf{Y} \nabla \mathbf{v} + \beta(\mathbf{I} - \nabla \mathbf{Y}).$$

Then by the identity  $\mathbf{I} = (\nabla \mathbf{Y})(\nabla \mathbf{Y})^{-1}$  and  $d\mathbf{I}/dt = 0$ , we can obtain  $d(\nabla \mathbf{Y}^{-1})/dt = (\nabla \mathbf{Y}^{-1})(d(\nabla \mathbf{Y})/dt)(\nabla \mathbf{Y}^{-1})$ , which gives the evolution of  $(\nabla \mathbf{Y})^{-1}$

$$\frac{\partial(\nabla \mathbf{Y})^{-1}}{\partial t} + \mathbf{v} \cdot \nabla(\nabla \mathbf{Y}^{-1}) = \nabla \mathbf{v} (\nabla \mathbf{Y})^{-1} + \beta(\mathbf{I} - \nabla \mathbf{Y}^{-1})(\nabla \mathbf{Y})^{-1}.$$

Using the generalized chain rule  $dJ/dt = [\partial J/\partial(\nabla \mathbf{Y})^{-1}] : [d(\nabla \mathbf{Y})^{-1}/dt]$  (where  $A : B = A_{ij}B_{ij}$  is the Frobenius inner product of two matrix represented in Einstein notation) and the formula  $\partial J/\partial(\nabla \mathbf{Y})^{-1} = J(\nabla \mathbf{Y})^T$ , we obtain the evolution of total volumetric change

$$\frac{dJ}{dt} = J[\nabla \cdot \mathbf{v} + \beta(d - \text{Tr}[\nabla \mathbf{Y}^{-1}])]. \quad (2)$$

**DERIVATION OF ELASTIC VOLUMETRIC CHANGE AND ISOTROPIC PRE-STRETCH**

Considering the decomposition of deformation tensor  $\nabla \mathbf{Y}^{-1} = \mathbf{F}_e \mathbf{P}$ , the prestrain tensor  $\mathbf{P} = \frac{\partial \mathbf{x}^*}{\partial \mathbf{y}}$  presents the transformation from the reference configuration ( $\mathbf{y} \in \Omega_0$ ) to a stress-free configuration ( $\mathbf{x}^* \in \Omega^*$ ) and the elastic deformation tensor  $\mathbf{F}_e = \frac{\partial \mathbf{x}}{\partial \mathbf{x}^*}$  presents the transformation from the stress-free configuration to the current deformed configuration ( $\mathbf{x} \in \Omega$ ). Consider the mass of tissue within an arbitrary domain  $\Omega$  in Eulerian coordinates at time  $t$  and use change of variable

$$\int_{\Omega} \rho(\mathbf{x}, t) d\mathbf{x} = \int_{\Omega^*} \rho(\mathbf{x}(\mathbf{x}^*), t) J_e d\mathbf{x}^* = \int_{\Omega_0} \rho(\mathbf{x}(\mathbf{y}), t) J d\mathbf{y},$$

where  $J_e = \det(\mathbf{F}_e)$  and  $J = \det(\nabla \mathbf{Y}^{-1})$  are the Jacobian determinant of the transformation  $\mathbf{F}_e$  and  $\nabla \mathbf{Y}^{-1}$ , respectively. On the other hand, the change of mass is only attributed to the volumetric change due to active growth  $J_g$  (that is, prestrain due to contractility and elastic deformation do not change the mass of a parcel of material in the flow)

$$\int_{\Omega} \rho(\mathbf{x}, t) d\mathbf{x} = \int_{\Omega^*} \rho_R d\mathbf{x}^* = \int_{\Omega_0} \rho_0 J_g d\mathbf{y},$$

---

\* [cwei4@wpi.edu](mailto:cwei4@wpi.edu)

† To whom correspondence should be addressed.  
E-mail: [englier@gmail.com](mailto:englier@gmail.com)

where  $\rho_R = \rho(\mathbf{x}^*, t)$  is the density in the stress-free configuration and  $\rho_0 = \rho(\mathbf{y}, 0)$  is the initial constant density in the reference configuration. Combining the above equations, we get the relations  $\rho J_e = \rho_R$  and  $\rho J = \rho_0 J_g$  for all the time  $t$ . Since  $J = J_e J_p = J_e J_g J_c$  due to the deformation decomposition, where  $J_c$  is the volumetric change due to active constriction, we have the relation  $\rho J_e J_c = \rho_R J_c = \rho_0 = \text{const.}$ , which yields

$$\frac{1}{\rho_R} \frac{d\rho_R}{dt} = -\frac{1}{J_c} \frac{dJ_c}{dt}, \quad \frac{1}{J_e} \frac{dJ_e}{dt} = -\frac{1}{\rho} \frac{d\rho}{dt} - \frac{1}{J_c} \frac{dJ_c}{dt}.$$

Introducing the rate of volume or area constriction  $\gamma_c = -(dJ_c/dt)/J_c$ , the stress-free tissue density will change by  $\dot{\rho}_R = \gamma_c \rho_R$ . Recall that the equation of mass conservation with the intrinsic growth rate  $\gamma$  gives

$$\frac{d\rho}{dt} = \rho(\gamma - \nabla \cdot \mathbf{v}).$$

We obtain the evolution of elastic volumetric change

$$\frac{dJ_e}{dt} = J_e(\nabla \cdot \mathbf{v} - \Gamma), \quad \text{where } \Gamma = \gamma - \gamma_c. \quad (3)$$

Moreover, combining the relation  $J_p = J/J_e$  and Eqs. 2 and 3, we get the evolution of isotropic pre-stretch

$$\frac{dJ_p}{dt} = J_p[\Gamma + \beta(d - \text{Tr}[\nabla \mathbf{Y}^{-1}])]. \quad (4)$$

## DERIVATION OF LINEARIZED MODEL

We will derive the linearized model in the limit of small deformation and fast tissue rearrangement. First, we consider the stress of the full nonlinear model represented in Eulerian coordinates

$$\begin{aligned} \boldsymbol{\sigma} &= \mu J_e^{-\frac{2+d}{d}} \left( \mathbf{F}_e \mathbf{F}_e^T - \frac{I_1}{d} \mathbf{I} \right) + K(J_e - 1) \mathbf{I}, \\ &= \mu J_p J^{-\frac{2+d}{d}} \left( \nabla \mathbf{Y}^{-1} \nabla \mathbf{Y}^{-T} - \frac{\tilde{I}_1}{d} \mathbf{I} \right) + K(J_p^{-1} J - 1) \mathbf{I}, \end{aligned}$$

where  $I_1 = \text{Tr}(\mathbf{F}_e^T \mathbf{F}_e)$  and  $\tilde{I}_1 = \text{Tr}(\nabla \mathbf{Y}^{-T} \nabla \mathbf{Y}^{-1})$  are the trace of the right Cauchy-Green *elastic* and *geometric* deformation tensors, respectively. By assuming that the displacement is small  $\mathbf{u} = \mathbf{x} - \mathbf{y}$ , i.e.,  $|\mathbf{u}| \sim O(\epsilon)$  and  $|\nabla \mathbf{u}| \sim O(\epsilon)$  with small parameter  $\epsilon$ , we have the following linearization

$$\begin{aligned} \nabla \mathbf{Y} &= \mathbf{I} - \nabla \mathbf{u}, \quad \nabla \mathbf{Y}^{-1} = \mathbf{I} + \nabla \mathbf{u}, \quad \nabla \mathbf{Y}^{-1} \nabla \mathbf{Y}^{-T} = \mathbf{I} + \nabla \mathbf{u} + \nabla \mathbf{u}^T \\ \det(\nabla \mathbf{Y}) &= 1 - \nabla \cdot \mathbf{u}, \quad \det(\nabla \mathbf{Y}^{-1}) = 1 + \nabla \cdot \mathbf{u}, \quad \tilde{I}_1 = d + 2\nabla \cdot \mathbf{u}. \end{aligned}$$

Further decomposing the accumulated pre-stretch change  $J_p = J_0(1+g)$  such that  $J_0 \sim O(1)$  is the global pre-stretch ( $J_0 = \text{const.}$ ) and  $g \sim O(\epsilon)$  is the differential pre-stretch, we obtain the linearized stress

$$\boldsymbol{\sigma} = \mu J_0 \left( \nabla \mathbf{u} + \nabla \mathbf{u}^T - \frac{2}{d} (\nabla \cdot \mathbf{u}) \mathbf{I} \right) + K J_0^{-1} \left( (1 - J_0) + (\nabla \cdot \mathbf{u} - g) \right) \mathbf{I}, \quad (5)$$

where the stress can be decomposed as  $\boldsymbol{\sigma} = \boldsymbol{\sigma}_s + \boldsymbol{\sigma}_p$ , the sum of the deviatoric part  $\boldsymbol{\sigma}_s$  (proportional to  $\mu$ ) and the isotropic part  $\boldsymbol{\sigma}_p$  (proportional to  $K$ ).

The leading-order linear approximation of Eq. 1 gives the evolution of the displacement

$$\frac{\partial \mathbf{u}}{\partial t} = \mathbf{v} - \beta \mathbf{u} \quad (6)$$

where the advection term is dropped as the higher order term of  $O(\epsilon)$ .

For the evolution of volumetric growth, we assume that the tissue rearrangement is faster than the active growth and constriction, i.e.,  $\Gamma/\beta \sim O(\epsilon)$ . The leading-order approximation of Eq. 4 gives

$$\frac{\partial g}{\partial t} = \Gamma - \beta \nabla \cdot \mathbf{u}. \quad (7)$$

Taking the time derivative of the stress Eq. 5 and using the evolution equations 6 and 7, we obtain the evolution of isotropic stress and deviatoric stress

$$\frac{\partial \boldsymbol{\sigma}_p}{\partial t} = \frac{K}{J_0} (\nabla \cdot \mathbf{v} - \Gamma) \mathbf{I}, \quad (8)$$

$$\boldsymbol{\sigma}_s + \frac{1}{\beta} \frac{\partial \boldsymbol{\sigma}_s}{\partial t} = \frac{\mu J_0}{\beta} \left( \nabla \mathbf{v} + \nabla \mathbf{v}^T - \frac{2}{d} (\nabla \cdot \mathbf{v}) \mathbf{I} \right). \quad (9)$$

## MODEL IN A 2D DISC

### Nonlinear Model

We first give the nonlinear model for a 2D disc in circular coordinates  $(r, \theta) \in \Omega = [0, R(t)] \times [0, 2\pi]$ . We further assume that the tissue is radially symmetric, in which case there is no displacement or velocity in circumferential direction nor the shear stresses, and the rest of solutions are functions of radius  $r$  and time  $t$  only. Introducing the displacement  $u = r - y$  and the velocity  $v$  in radial direction, the resultant nonlinear system is

$$\begin{aligned}\frac{\partial u}{\partial t} + v \frac{\partial u}{\partial r} &= v - \beta u, \\ \frac{\partial J_p}{\partial t} + v \frac{\partial J_p}{\partial r} &= J_p \left[ \Gamma + \beta \left( 2 - \left( \frac{\partial y}{\partial r} \right)^{-1} - \left( \frac{y}{r} \right)^{-1} \right) \right], \\ \alpha v &= \frac{\partial \sigma_{rr}}{\partial r} + \frac{1}{r} (\sigma_{rr} - \sigma_{\theta\theta}),\end{aligned}$$

where the stress is

$$\begin{aligned}\sigma_{rr} &= \frac{1}{2} \mu J_p \left[ \left( \frac{y}{r} \right)^2 - \left( \frac{\partial y}{\partial r} \right)^2 \right] + K \left( J_p^{-1} \left( \frac{\partial y}{\partial r} \right)^{-1} \left( \frac{y}{r} \right)^{-1} - 1 \right), \\ \sigma_{\theta\theta} &= \frac{1}{2} \mu J_p \left[ \left( \frac{\partial y}{\partial r} \right)^2 - \left( \frac{y}{r} \right)^2 \right] + K \left( J_p^{-1} \left( \frac{\partial y}{\partial r} \right)^{-1} \left( \frac{y}{r} \right)^{-1} - 1 \right).\end{aligned}$$

subject to the deformation-free initial condition

$$y(r, 0) = r, \quad J_p(r, 0) = J_0$$

with the initial pre-stretch  $J_0$  and the corresponding moving boundary conditions

$$\sigma_{rr}(R, t) = K(J_0^{-1} - 1), \quad \frac{dR}{dt} = v(R, t).$$

We perform numerical simulations for the above nonlinear system for  $J_0 = 1$  without loss of generality. The nonlinear system is numerically solved by an implicit iterative method, where the moving boundary condition is dealt with by the rescaling of radius  $r' = r/R(t) \in [0, 1]$  in a fixed domain. The details of the numerical method is not the core of this paper and will be presented in a substantial paper in near future on its own right.

### Linear Model

Assuming  $u = r - y$  and  $J_p = J_0(1 + g)$  with small  $u$ ,  $\partial_r u$  and  $g$ , the linearized model in 2D Disc is

$$\begin{aligned}\frac{\partial u}{\partial t} &= v - \beta u, \\ \frac{\partial g}{\partial t} &= \Gamma - \beta \left( \frac{\partial u}{\partial r} + \frac{u}{r} \right), \\ \alpha v &= \frac{\partial \sigma_{rr}}{\partial r} + \frac{1}{r} (\sigma_{rr} - \sigma_{\theta\theta}),\end{aligned}$$

where the stress is

$$\begin{aligned}\sigma_{rr} &= \mu J_0 \left( \frac{\partial u}{\partial r} - \frac{u}{r} \right) + K J_0^{-1} \left( \frac{\partial u}{\partial r} + \frac{u}{r} - g \right) + K(J_0^{-1} - 1), \\ \sigma_{\theta\theta} &= \mu J_0 \left( \frac{u}{r} - \frac{\partial u}{\partial r} \right) + K J_0^{-1} \left( \frac{\partial u}{\partial r} + \frac{u}{r} - g \right) + K(J_0^{-1} - 1),\end{aligned}$$

subject to initial conditions

$$u(r, 0) = 0, \quad g(r, 0) = 0$$

and boundary conditions

$$\sigma_{rr}(R, t) = K(J_0^{-1} - 1), \quad \frac{dR}{dt} = v(R, t).$$

The analytical steady-state solutions of the linear system is given by Eqs. (15) and (16) in the main text.

### NONLINEAR EFFECT ON TISSUE SIZE

To understand the variation in tissue size modulated by  $K$  and  $\beta$ , we consider the rate of change of  $J_e$  in the Eulerian coordinates. When the tissue is at mechanical equilibrium, we have  $\partial_t J_e = J_e(\nabla \cdot \mathbf{v} - \Gamma) - \mathbf{v} \cdot \nabla J_e = 0$ . If we consider the integral of  $(\partial_t J_e)/J_e$  over a subregion in the tissue ( $A \subset \Omega$ ), we can derive

$$\int_{\partial A} (\mathbf{v} \cdot \mathbf{n}) dS = \int_A (\nabla \cdot \mathbf{v}) dV = \int_A \left( \Gamma + \frac{1}{J_e} (\mathbf{v} \cdot \nabla J_e) \right) dV, \quad (10)$$

where we use the divergence theorem for the first equality and  $\mathbf{n}$  is the unit outward normal vector of the boundary  $\partial A$ . This equation shows that the local expansion/contraction is the result of the competition between the intrinsic active growth and constriction (independent on the flow) and the advection in tissue flow. When we consider the equation in the whole tissue  $\Omega$ , the velocity at boundary is zero,  $\mathbf{v} = 0$  at  $\partial\Omega$ , and we have the relation that determines tissue equilibrium size

$$\int_{\Omega} \Gamma dV = - \int_{\Omega} \frac{1}{J_e} (\mathbf{v} \cdot \nabla J_e) dV, \quad (11)$$

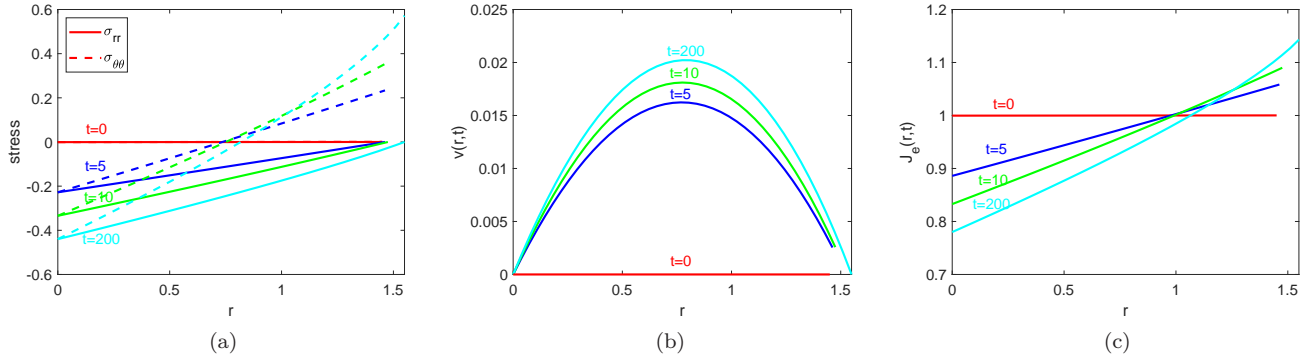


FIG. 1. The dynamics of (a) mechanical stresses, (b) tissue flow velocity  $v$  and (c) the inverse of cell density  $J_e$ , corresponding to the tissue growth for  $\beta = 0.2$  and  $K = 2$  in Fig. 2 in the main text.

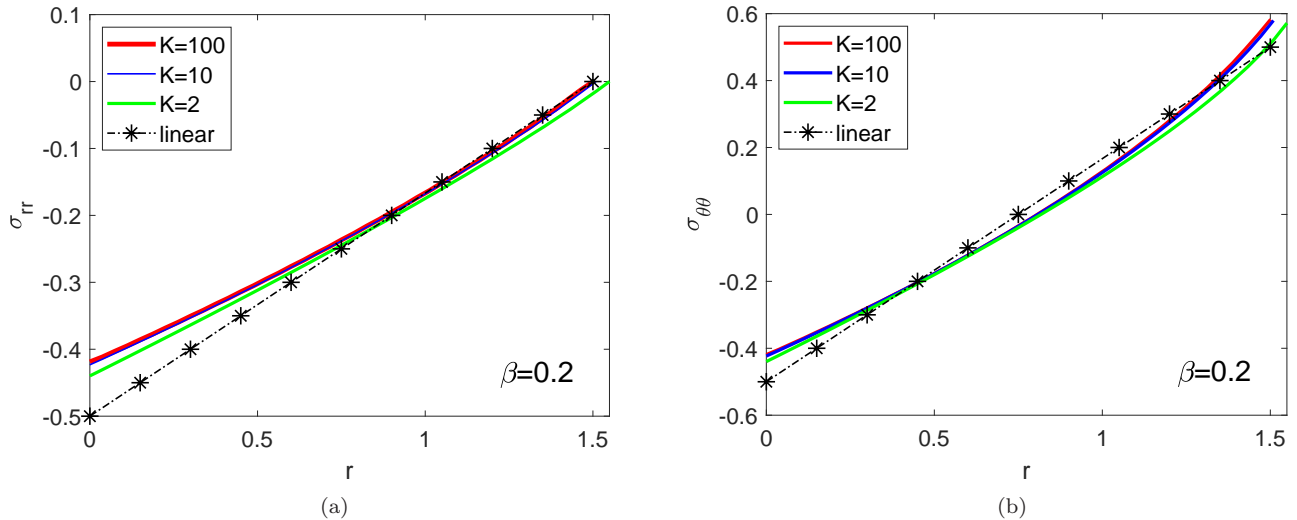


FIG. 2. (a) Radial stress  $\sigma_{rr}$  and (b) circumferential stress  $\sigma_{\theta\theta}$  for fixed  $\beta = 0.2$  and different  $K = 2, 10, 100$ , corresponding to the steady states c, d and e in Fig. 2 in the main text. Solid lines represent results from nonlinear simulations and dash-star line represents the linear analytical solution.

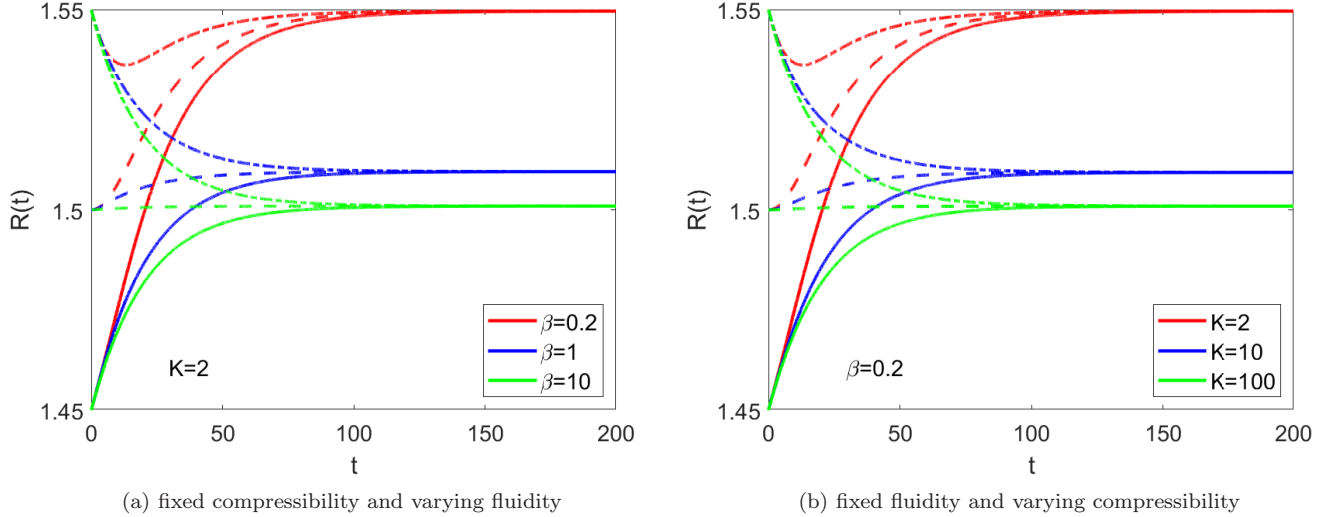


FIG. 3. Evolution of tissue size  $R(t)$  with different initial sizes for (a)  $K = 2$  and  $\beta = 0.2, 1, 10$  and (b)  $\beta = 0.2$  and  $K = 2, 10, 100$ . Solid lines starts with initial size  $R = 1.45$ , dash lines with  $R = 1.5$  and dash-dot lines with  $R = 1.55$ . The equilibrium size is independent on the initial size and only dependent on the tissue properties  $K$  and  $\beta$ .

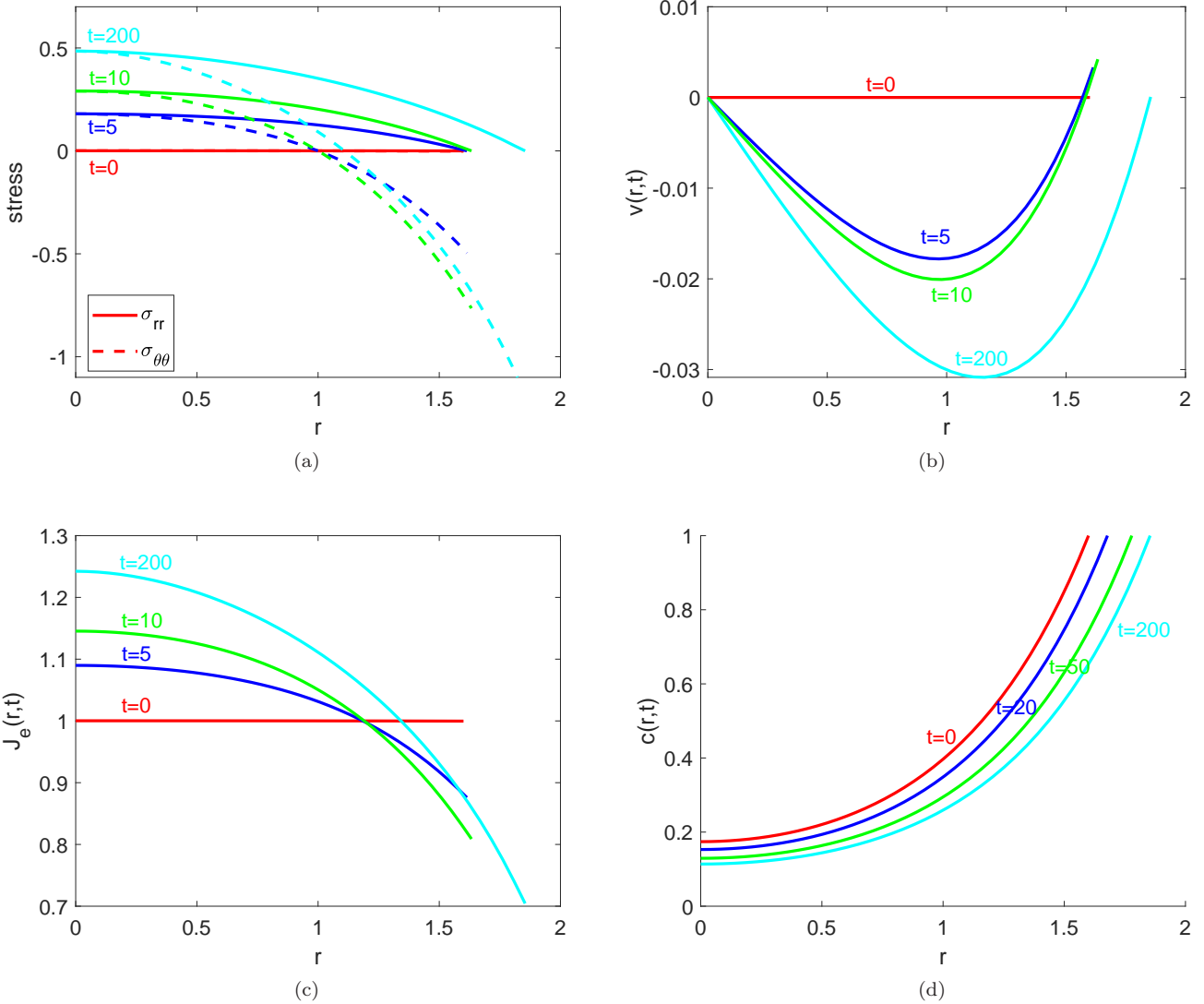


FIG. 4. The dynamics of (a) mechanical stresses, (b) tissue flow velocity  $v$ , (c) the inverse of cell density  $J_e$ , coupled with the reaction-diffusion process of (d) the concentration of growth factor  $c$ , corresponding to the tissue growth for  $\beta = 0.2$  and  $K = 2$  in Fig. 3 in the main text.

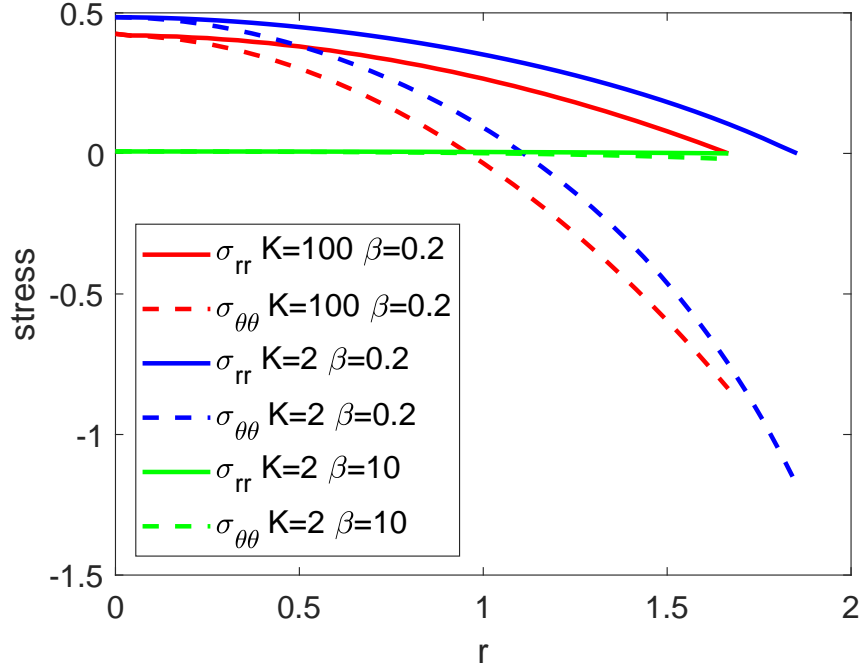


FIG. 5. Radial stress  $\sigma_{rr}$  (solid lines) and circumferential stress  $\sigma_{\theta\theta}$  (dash lines), corresponding to the steady states a ( $K = 100, \beta = 0.2$ ), b ( $K = 2, \beta = 0.2$ ) and c ( $K = 2, \beta = 10$ ) in Fig. 3 in the main text. The magnitudes of both stresses are smaller for incompressible tissue  $K = 100$  than compressible tissue  $K = 2$ . The stresses vanish for large tissue fluidity  $\beta = 10$ .

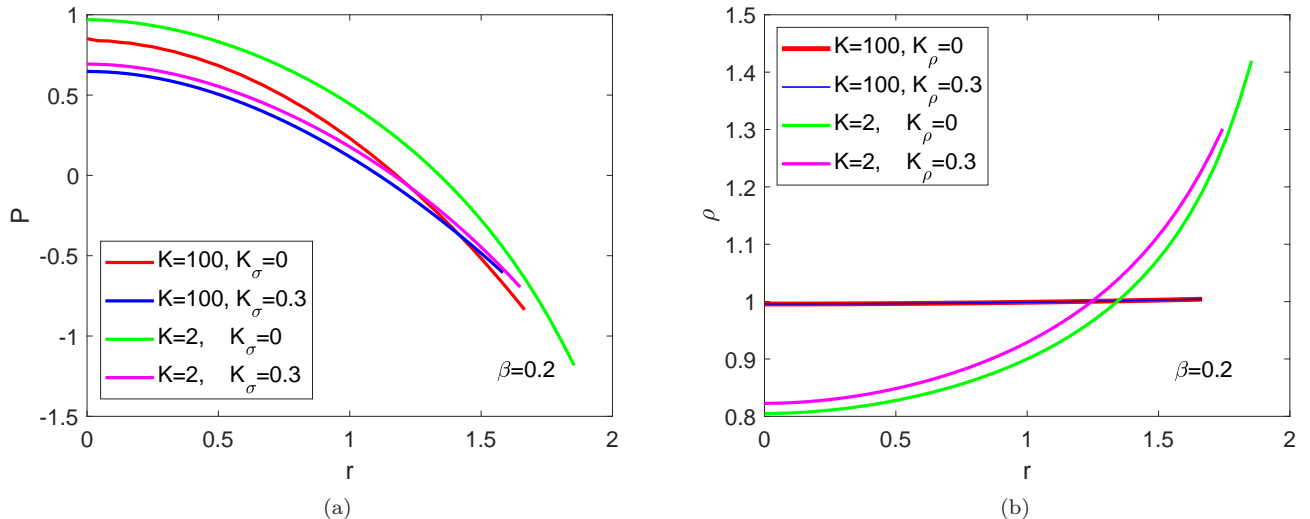


FIG. 6. (a) Pressure  $P = \sigma_{rr} + \sigma_{\theta\theta}$  with ( $K_\sigma = 0.3$ ) or without ( $K_\sigma = 0$ ) stress-induced mechanical feedback, for different compressibility  $K$ . Both the absolute magnitude of pressure and the relative change of pressure due to stress-induced feedback are larger for compressible tissue  $K = 2$  than for incompressible tissue  $K = 100$ . (b) Cell density distribution  $\rho$  with ( $K_\rho = 0.3$ ) or without ( $K_\rho = 0$ ) contact-inhibition mechanical feedback, for different compressibility  $K$ . There is no variation in cell density for incompressible tissue  $K = 100$  regardless of the effect of contact-inhibition feedback.